Available online at www.sciencedirect.com
ScienceDirect
Scripta Materialia 63 (2010) 1220–1223
Scripta MATERIALIA
www.elsevier.com/locate/scriptamat

Damage observation in a high-manganese austenitic TWIP steel by synchrotron radiation computed tomography

J. Lorthios,[a,*] F. Nguyen,[a] A.-F. Gourgues,[a] T.F. Morgeneyer[a] and P. Cugy[b]

[a] *Mines Paristech, Centre des Matériaux, UMR CNRS 7633, BP87 91003 Evry cedex, France*
[b] *ArcelorMittal Research, Voie Romaine-BP30320, 57283 Maizières-lès-Metz cedex, France*

Received 9 July 2010; revised 19 August 2010; accepted 20 August 2010
Available online 25 August 2010

Internal damage below the fracture surface of a multiaxial specimen made of twinning-induced plasticity (TWIP) steel was observed by three-dimensional X-ray microtomography as very elongated "primary" voids. Specific tools for the local damage analysis were developed. A gradient in void volume fraction was measured from the fracture surface down to the bulk of the scanned volume (from ~0.06% to <0.02%). However, the fracture surface is mainly composed of tiny secondary dimples (>90% in area fraction), indicating strongly localized final fracture.

Keywords: TWIP steel, X-ray synchrotron radiation; Fracture; Anisotropic damage development

High-manganese austenitic steels have been produced in cold-rolled format for the automotive industry; they offer great potential for body weight reduction combined with impact resistance. In fact, tensile strength levels higher than 1000 MPa in combination with a high ductility (>40%) have been achieved by controlling the microstructure and deformation mechanisms. Hence, the steel is fully austenitic at room temperature and deformation occurs by mechanical twinning (in addition to planar dislocation glide), inducing twinning-induced plasticity (TWIP) [1–2].

These so-called TWIP steels exhibit an unusually high work-hardening capacity, the underlying mechanism of which is still a subject of controversy [3–5]. The complex interactions between dislocations and the relaxation mechanisms result in a high elongation capacity. While the fracture surface is fully ductile, slant fracture occurs, though without appreciable necking, and the material seems to be sensitive to shear fracture.

In the automotive industry, the evaluation of forming performance and the prediction of shear fracture have become important issues. For this fracture mode, the straining limits are not set by classical necking criteria and standard analyses based on the forming limit diagram cannot be used to evaluate forming performance. Hence, formability limits must be identified by other means. For example, Hudgins et al. [6] looked for critical die and punch radii in bending under tension and stretch forming in order to produce shear failure similar to that encountered during stamping of several advanced high-strength steels (AHSSs), namely high-strength low-alloy, dual-phase and transformation-induced plasticity-aided steels. These values have been used as a measurement of the forming performance. TWIP steels are austenitic steels with ultimate tensile strengths similar to those of AHSSs. However, their fracture behavior differs from that of AHSSs because shear fracture is encountered in a variety of loading modes, i.e. for widely different levels of stress and strain triaxiality ratio. Until now, fracture and damage mechanisms in TWIP steels have been poorly understood and nothing on this subject has been reported in the open literature.

The present paper addresses the investigation of damage below the fracture surface of a broken specimen. For the first time, a sample of fractured FeMn TWIP steel was investigated using synchrotron radiation computed tomography. This imaging technique enables the visualization of internal features of the sample in three dimensions and highlights the existence of damage [7], as previously detected in a dual-phase steel by Maire et al. [8]. Qualitative and quantitative information extracted from the three-dimensional image will permit assessment of both the spatial extension of the damaged area and representative size distribution and volume fraction of damage.

* Corresponding author. Tel.: +33 160763045; fax: +33 160763150; e-mail: julie.lorthios@ensmp.fr

1359-6462/$ - see front matter © 2010 Acta Materialia Inc. Published by Elsevier Ltd. All rights reserved.
doi:10.1016/j.scriptamat.2010.08.042

The study focuses on a recrystallized Fe–Mn–C steel containing 0.6 wt.% C and 22 wt.% Mn, provided by ArcelorMittal. The sheet had been cold-rolled down to 1.5 mm in thickness and then annealed, leading to equiaxed γ grains (2–3 μm in size) with a weak texture (texture index 1.23).

An experimental database was gathered to characterize the flow behavior of the material and to examine any anisotropy effects on both plasticity and fracture at room temperature. Tensile tests along the rolling, transverse and 45° directions of the sheet were carried out on dogbone specimens (gauge length: 60 mm, width: 12.5 mm). The Lankford coefficients were obtained directly via measuring the deformation on the specimen after fracture (far from the necking area) and were compared to strain fields obtained by digital image correlation (DIC) during the tensile tests. Fracture surfaces of the specimens were observed using scanning electron microscopy (SEM).

However, the sensitivity of the material to shear fracture encouraged us to study damage under shear loading conditions. Thus, the geometry of the specimen investigated in detail in the present experimental work was taken from the study of Brünig et al. [9]. This "butterfly" geometry, shown in Figure. 1a, conveniently concentrates shear stresses within the middle part of the specimen while using a uniaxial tensile machine. The specimen was loaded in tension along the rolling and the transverse direction of the sheet. In order to analyze the experiment, strain and stress fields were simulated using a finite-element model. Constitutive equations of the material were identified from the experimental database, consisting of tensile and shear tests [10]. The numerical results were validated by comparison with measurements of the strain fields obtained by DIC.

A "butterfly" specimen loaded along the rolling direction was chosen to investigate damage below the fracture area using X-ray microtomography. Localization of deformation to a small part of the specimen increases the chance of observing a significant damage gradient in the small scanned volume investigated using synchrotron radiation. A sample 250 × 250 × 2000 μm in size was cut below the fracture surface of the broken "butterfly" specimen by spark electrical discharge machining (Fig. 2b). It exhibits a tapered shape corresponding to the inclination of the fracture surface with respect to the specimen axes.

Damage in the bulk of the sample was investigated using X-ray microtomography at the ID-19 beamline of the European Synchrotron Radiation Facility (Grenoble). The energy was set to 40 keV and the voxel size is 0.7 μm. The size of the scanned volume is 250 × 250 × 1420 μm. A scan consisting of 1500 projections was acquired. Phase-contrast imaging was used to detect small damage features. Further details on the technique may be found in Ref. [7].

A thresholding procedure based on morphological mathematics was chosen rather than classical thresholding methods directly based on gray-scale histograms, because the size of the microstructural objects to be extracted is small, as will be shown below. Hence, the objects were considered using local gray-scale minima in the image. Each object was thus individually described as a group of voxels surrounded by higher gray-scale voxels. With this technique—and irrespective of the overall contrast of the 3-D image due to non-uniform sample thickness near the tapered edge—damage and its associated voids could be distinguished from the rest of the investigated volume. Moreover, in order to investigate only damage that was not connected to the fracture surface, all voids connected in 3-D with the fracture surface were removed from analysis.

The results of the uniaxial tensile tests on dogbone specimens showed that the material exhibits an ultimate tensile strength of 1100 MPa and 45% elongation at fracture. The initial yield strength reaches 590 MPa.

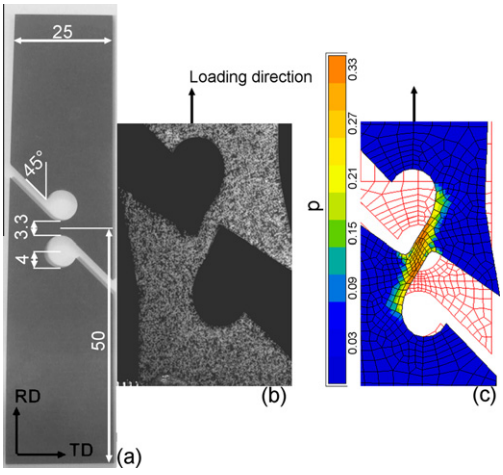

Figure 1. Geometry of the "butterfly" specimen (a) unstrained (all dimensions in mm), (b) at fracture (closer view), (c) based on fracture–strain field modeling (cumulative plastic strain).

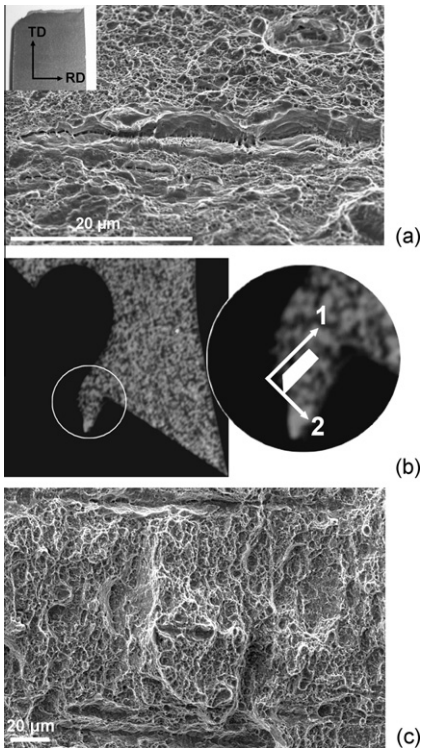

Figure 2. (a) Fracture surface of a tensile specimen loaded along the transverse direction, (b) macroscopic shape and (c) fracture surface of the broken "butterfly" specimen (tomography sample schematically drawn in white).

The mean reduction of area, measured directly on the specimen in the fracture area, is almost 38%. The values of the Lankford coefficients—0.80 for tension along the rolling direction and 1.35 along the transverse direction—reveal anisotropy of plastic flow.

As seen in Figure. 1b, the shear "butterfly" specimen exhibits a large amount of strain just before fracture and a high rotation (almost 47°) of the strained area. According to the strain fields from the DIC measurements, local strain reaches 40% in the fracture area. Simulation of the strain field at the moment of fracture, superimposed on the initial mesh (in red in Fig. 1c) yields good agreement with DIC measurements, suggesting that the loading mode can be analyzed using finite-element simulation. This shows that the loading mode evolves from shear to almost uniaxial tension along the loading direction at the end of the experiment, because of the high ductility of the steel. The maximum triaxiality ratio reaches 1/3 in uniaxial tension, and it may be expected that void growth will be limited. The broken butterfly specimen is shown in Figure. 2b. Examination of the rolling marks directly on the specimen surface indicates that the fracture surface direction is close to the rolling direction.

Fracture surfaces of a tensile (Fig. 2a) and of the shear "butterfly" specimen (Fig. 2c) were observed using SEM, and revealed a ductile fracture mode with microvoids less than 1 μm in size that cannot be captured using X-ray microtomography under the conditions used here. Larger voids, apparently free of coarse secondary phases or inclusions, were also observed. These voids are elongated along the rolling direction (irrespective of the orientation of the tensile axis with respect to the sheet). Several cross-sections of tensile broken specimens were then prepared using standard metallographic methods and observed using SEM in order to link these elongated voids with underlying damage. However, no void could be evidenced with this technique.

As shown in Figure. 3a, the 3-D image resulting from X-ray microtomography reveals the existence of damage below the fracture surface, which (to the authors' knowledge) had not previously been evidenced for this material. Internal damage seems to be organized as stringers of voids with a preferential elongation along a direction that is not parallel to either of the 1, 2 or 3 axes of the "butterfly" specimen.

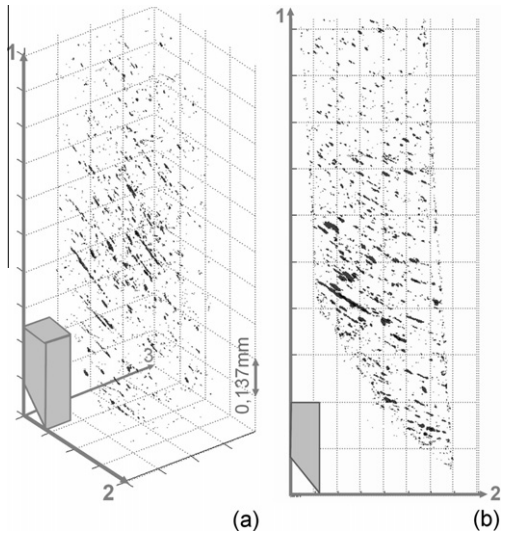

Figure 3. (a) 3-D X-ray microtomograph image of the internal damage (tomography sample schematically drawn in gray); (b) 2-D projection of the damage in the [1,2] frame.

An orthogonal projection of the 3-D image in the [1,2] plane (Fig. 3b) is a convenient representation to identify the direction of elongation of the voids in relation to the fracture surface. (Nevertheless this representation overestimates the apparent volume fraction since all the voids of the volume have been integrated into a single 2-D section.) The voids tend to be parallel to the fracture surface and are elongated along the rolling direction.

The volume fraction of voids, measured over the whole investigated volume, is low: 0.035%. In order to assess the damage gradient below the fracture surface, the volume fraction of voids was then measured, from the fracture surface to the bulk of the analyzed volume (Fig. 4a) along the 1 axis, slice by slice parallel to the fracture surface (thick red[1] lines in Fig. 4a; slice thickness 7 μm). Damage was observed until up to 1 mm below the fracture surface. Despite scatter, far from the fracture surface (and thus also near the undeformed material), the volume fraction of voids can be considered to be lower than 0.02%. Thus, even if no direct measurement was made, the porosity of the initial material seems to be close to zero. The volume fraction of voids is higher closer to the fracture surface, about 0.06% on average. However, it remains very low (in comparison, the volume fraction of voids in a dual-phase steel specimen broken in tension at room temperature reaches 2% [8]). Bulk damage in TWIP steels exists as primary cavities but this low volume fraction explains why very few voids were observed using SEM of cross-sections.

The use of global damage analysis tools, such as 3-D covariance and fast Fourier transformation (FFT), did not provide any meaningful results due to the low void volume fraction and the small material volume investigated.

A local approach was thus favored in order to assess the size distribution of voids and to compare internal voids to the dimples observed on fracture surfaces. To this aim, the principal lengths and the volume of each void were measured. In the literature, voids are often described by their orthogonal projection length (the Feret projection) along the directions of a fixed coordinate system. However, this method cannot be applied when the voids are inclined at angles that vary in 3-D terms, as is the case here. A more precise method using an ellipsoid approximation of the shape of each void was thus chosen. For each void, the inertia matrix of the set of voxels belonging to that void was computed and the three principal axes of the ellipsoid were deduced from the eigenvalues of this matrix. This method gives no error on the principal axis of the ellipsoid, which is exactly the principal length of that particular void.

The size distribution of voids (Fig. 4b) shows that the majority of the voids were very small and their volume did not exceed a few voxels, i.e. a few times $3 \times 10{-}6$ mm^3. Several larger voids were, however, identified close to the fracture surface. Two of these are shown in Figure.

[1] For interpretation of color in Figs. 4-6, the reader is referred to the web version of this article.

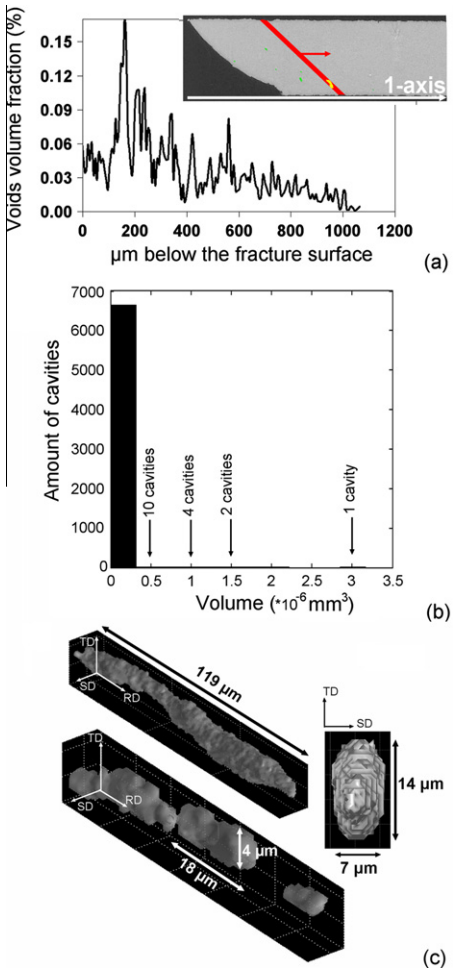

Figure 4. (a) Void volume fraction measured in 7 µm thick slices 45° inclined to the 1 axis and (b) volume distribution of voids. (c) 3-D view of two voids extracted from the 3-D image and 2-D view of one of them along the (TD, SD) plane.

4c. The upper void in Figure. 4c, extracted from the 3-D image, is the longest void found in the investigated volume; it achieves more than 100 µm in length along the rolling direction. The presence of large voids in the bulk of the specimen indicates that these are "primary" voids that nucleate and grow prior to final fracture. The bottom void in Figure. 4c is representative of alignments of smaller voids found in the bulk of the sample. This void may stem from the coalescence of two smaller voids, each of the order of microns in size. As the longest axis of the void was identified to be parallel to the rolling direction, the transverse (TD) and short transverse direction (SD) of the sheet are known with respect to the void axes. Observation of sections of such voids in the [TD, SD] plane (e.g. upper right in Fig. 4c) revealed that they are not circular but elliptic. The size of this particular void along the TD direction varies from 4 up to 14 µm, whereas it reaches up to 7 µm along the SD direction. In fact, the ratio between the length along TD and the length along SD, respectively, is 1.73 on average (calculated on [TD,SD] void slices with a surface area higher than 10 pixels) with a standard deviation of 0.35. This observation is coherent with the plastic flow anisotropy revealed by the Lankford coefficients for uniaxial tension along the rolling direction (0.80). In fact, under low stress triaxiality (~1/3 at the end of the test from finite-element simulations), and thus with a low growth rate, deformation of voids is dictated by that of the surrounding material. Thus, under tension along RD, as the material will "shrink" more along SD than along TD, the voids tend to be larger along TD than along SD. Unit cell finite-element calculations for this material under uniaxial tension, based on the low triaxiality ratio assumption (i.e. assuming no void growth), confirmed this point.

The larger internal voids revealed by local X-ray microtomography analysis (e.g. Fig. 4c) are of the same size and spatial orientation as those observed in fracture surfaces (Fig. 2). All these voids have their long axis parallel to the rolling direction. Thus, locally, damage first appears as numerous strings of small voids, merging into larger "primary" voids. Their growth up to a size of more than ~10 µm shows that bulk damage initiation probably begins well before the occurrence of fracture, but is not immediately followed by the specimen failure (i.e. no decrease in load is observed even in uniaxial tension). Hence, these large "primary" voids do not directly lead to final fracture. Moreover, as shown previously, the fracture surfaces are mainly comprised of microvoids less than 0.5 µm in size. These are not visible by X-ray microtomography because the spatial resolution of 0.7 µm in voxel size is not sufficient. Final fracture is sudden and is characterized by the nucleation and early coalescence of these "secondary" microvoids. The underlying mechanism is still to be explored.

For the first time, to the authors' knowledge, X-ray microtomography has highlighted the existence of bulk damage adjacent to the fracture area of a TWIP steel specimen and up to 1000 µm below the fracture surface. Large, but scarce, strings of voids elongated along the rolling direction were evidenced using tomography, but could not be revealed with conventional metallography. The small volume fraction and the varying orientation of these "primary" voids with respect to the loading axis have enabled us to successfully develop specific data processing of the 3-D image. Local quantitative analysis revealed the anisotropic growth of those voids, in agreement with the Lankford coefficients.

The authors would like to acknowledge Elodie Boller, at the ID19 beamline at ESRF, and Henry Proudhon from MINES ParisTech for help with synchrotron radiation tomography.

[1] L. Rémy, Acta Metall. 26 (1978) 443–451.
[2] O. Grassel, L. Kruger, G. Frommeyer, L.W. Meyer, Int. J. Plast. 16 (2000) 1391–1409.
[3] O. Bouaziz, S. Allain, C. Scott, Scr. Mater. 58 (2008) 484–487.
[4] B. Hutchinson, N. Ridley, Scr. Mater. 55 (2006) 299–302.
[5] Y.N. Dastur, N. Leslie, A. Met. Trans. 12A (1981) 749–759.
[6] A. Hudgins, D. Matlock, J. Speer, J. Fekete, M. Walp, Mater. Sci. Technol. 1 (2007) 143–155.
[7] E. Maire, J.-Y. Buffière, L. Salvo, J.J. Blandin, W. Ludwig, J.M. Letang, Adv. Eng. Mater. 3 (2001) 539–546.
[8] E. Maire, O. Bouaziz, M. Di Michiel, C. Verdu, Acta. Mater. 56 (2008) 4954–4964.
[9] M. Brünig, O. Chyra, D. Albrecht, L. Driemeier, M. Alves, Int. J. Plast. 24 (2008) 1731–1755.
[10] J. Lorthios, Internal report, ArcelorMittal, 2009.